Sixth International Symposium on Turbulence and Shear Flow Phenomena
Seoul, Korea, 22-24 June 2009

NEAR-WALL BEHAVIORS OF TURBULENT HYDROGEN/AIR AND METHANE/AIR PREMIXED FLAMES

Akihiko Tsunemi, Mamoru Tanahashi and Toshio Miyauchi
Department of Mechanical and Aerospace Engineering,
Tokyo Institute of Technology
2-12-1 Ookayama, Meguro-ku, Tokyo 152-8550, Japan
atsunem@navier.mes.titech.ac.jp, mtanahas@mes.titech.ac.jp, tmiyauch@mes.titech.ac.jp

Makoto Nagaoka
Toyota Central R&D Labs.,
41-1 Aza Yokomichi, Oaza Nagakute, Nagakute-cho, Aichi-gun, Aichi 480-1192, Japan
nagaoka@mosk.tytlabs.co.jp

ABSTRACT

Direct numerical simulations (DNSs) of interactions between turbulent premixed flame and isothermal wall have been conducted to investigate heat losses and quenching mechanism of turbulent premixed flames near the wall. Near-wall behaviors of hydrogen/air and methane/air premixed flames were investigated by considering detailed kinetic mechanism. For hydrogen/air flame, heat release rate in near-wall region is higher than that of freely-propagating flame. For methane/air flame, however, heat release rate near the wall becomes lower than that of freely-propagating flame. This difference is caused by different contributions of certain low-temperature reactions that are enhanced near the wall to the total heat release rate. The wall heat flux of hydrogen/air turbulent flame is higher than that of corresponding laminar flame, because the turbulent burning velocity increases significantly and pressure rises near the flame region. For methane flame, however, the wall heat flux nearly coincides with that of laminar flame since the turbulent burning velocity is not enhanced due to local extinction.

INTRODUCTION

The flame-wall interaction is important for the efficiency of many combustors in engineering applications, whereas details of that have not been clarified yet. As for the flame-wall interaction, several researches have been reported for hydrogen flame and methane flame (Dabireau et al., 2003; Owston et al., 2007; Popp and Baum, 1997). In general, the flame-wall interaction can be classified into head-on quenching (HOQ) and side-wall quenching (SWQ). Dabireau et al. (2003) have conducted numerical simulation of HOQ flame-wall interaction of H_2/O_2 premixed and non-premixed laminar flame with a detailed kinetic mechanism. They have shown that H_2/O_2 premixed flame shows high heat flux just before the flame impinging to the wall. Owston et al. (2007) have extended the similar HOQ simulation to investigate effects of wall temperature, pressure, equivalence ratio and diluents, for hydrogen flames. As for hydrocarbon flame, Popp and Baum (1997) have analyzed wall temperature effects on the near-wall behaviors of laminar methane flame. Near wall behavior of the flame has also been investigated experimentally (Bellenoue et al., 2003; Boust et al., 2007). In experiments, the information obtained has been limited to global character of the flame such as quenching distance. Most of numerical and experimental studies are limited to a laminar flow. Since the flow in engineering applications is in turbulent state, investigation on flame-wall interaction in turbulence field is required.

In this study, direct numerical simulations of interactions between turbulent premixed flame and isothermal wall have been conducted to investigate heat losses and quenching mechanism of turbulent premixed flames near the wall by considering detailed kinetic mechanism.

DIRECT NUMERICAL SIMULATION

Figure 1 shows schematic of the numerical configuration. The geometry of combustion field is the ignition of turbulent premixed mixture between two parallel walls in two dimensions. The governing equations are conservation equations of mass, momentum, energy and species concentration. Details of the governing equations have been shown by Miyauchi et al. (1996). In this study, Soret effect, Dufour effect, pressure gradient diffusion, bulk viscosity and radiative heat transfer are assumed to be negligible and DNS code developed in our previous studies (Tanahashi et al., 2000; Tanahashi et al., 2002) is modified for wall-bounded flows. Spatial discretization is conducted by fourth order central finite difference scheme, and fourth order compact finite difference filter (Lele, 1992) is considered. Time integration is implemented by a third order Runge-Kutta scheme. Reaction source terms in species conservation equations are implemented by an implicit method (Brown et al, 1989). The length of walls is 40 mm and the gap between the walls is 5 mm. Preheating temperature is set to 700K and wall temperature (T_{wall}) is set to 700K or 450K. Equivalence ratio and pressure are set to 1.0 and 0.1MPa, respectively. The DNSs are conducted with 2049×257 grid points.

The boundary conditions at the walls are isothermal no-slip wall (Poinsot and Lele, 1992; Baum et al., 1994) and wall surfaces are supposed to be chemically inert. Those in the other direction are non-reflecting outflow conditions given by Navier-Stokes characteristic boundary condition (NSCBC) (Poinsot and Lele, 1992; Baum et al., 1994). Detailed kinetic mechanism including 12 reactive species and 27 elementary reactions is used for hydrogen/air mixture. This detailed kinetic mechanism has been picked up from Miller and Bowman (1991), Smooke and Giovangigli (1991), Kee et al. (1996) as shown in Table 1. For methane/air mixture,

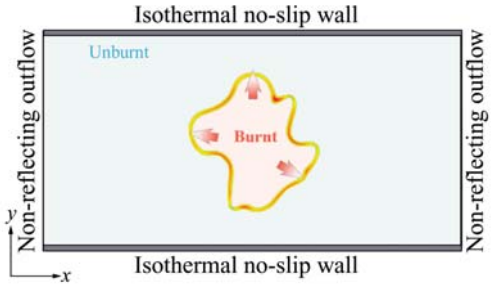

Figure 1: Geometry of the flow field.

Table 1: Detailed kinetic mechanism for hydrogen/air mixture. (A: frequency factor, β: pre-exponential temperature exponent, E: activation energy)

No.	Reaction	A	β	E
1f	$H+O_2 \Rightarrow OH+O$	2.00e+14	0	16800
1b	$OH+O \Rightarrow H+O_2$	1.58e+09	0	690
2f	$H_2+O \Rightarrow OH+H$	1.80e+10	1	8826
2b	$OH+H \Rightarrow H_2+O$	8.00e+09	1	6760
3f	$H_2+OH \Rightarrow H_2O+H$	1.17e+09	1.3	3626
3b	$H_2O+H \Rightarrow H_2+OH$	5.09e+09	1.3	18588
4f	$OH+OH \Rightarrow O+H_2O$	6.00e+08	1.3	0
4b	$H_2O+O \Rightarrow OH+OH$	5.90e+09	1.3	17029
5	$H_2+O_2 \Leftrightarrow OH+OH$	1.70e+14	0	47780
6	$H+O_2+M \Leftrightarrow HO_2+M$ $H_2O/18.6/$ $H_2/2.9/$ $N_2/1.3/$	3.61e+17	-0.72	0
7	$OH+HO_2 \Leftrightarrow H_2O+O$	7.50e+12	0	0
8	$H+HO_2 \Leftrightarrow OH+OH$	1.40e+14	0	1073
9	$O+HO_2 \Leftrightarrow O_2+OH$	1.40e+13	0	1073
10	$H+H+M \Leftrightarrow H_2+M$ $H_2O/0.0/$ $H_2/0.0/$	1.00e+18	-1	0
11	$H+H+H_2 \Leftrightarrow H_2+H_2$	9.20e+16	-0.6	0
12	$H+H+H_2O \Leftrightarrow H_2+H_2O$	6.00e+19	-1.25	0
13	$H+OH+M \Leftrightarrow H_2O+M$ $H_2O/5.0/$	1.60e+22	-2	0
14	$H+O+M \Leftrightarrow OH+M$ $H_2O/5.0/$	6.20e+16	-0.6	0
15	$O+O+M \Leftrightarrow O_2+M$	1.89e+13	0	-1788
16	$H+HO_2 \Leftrightarrow H_2+O_2$	1.25e+13	0	0
17	$HO_2+HO_2 \Leftrightarrow H_2O_2+O_2$	2.00e+12	0	0
18	$H_2O_2+M \Leftrightarrow OH+OH+M$	1.30e+17	0	45500
19	$H_2O_2+H \Leftrightarrow HO_2+H_2$	1.60e+12	0	3800
20	$H_2O_2+OH \Leftrightarrow H_2O+HO_2$	1.00e+13	0	1800
21	$N+NO \Leftrightarrow N_2+O$	3.27e+12	0.3	0
22	$N+O_2 \Leftrightarrow NO+O$	6.40e+09	1	6280
23	$N+OH \Leftrightarrow NO+H$	3.08e+13	0	0
24	$HO_2+NO \Leftrightarrow NO_2+OH$	2.11e+12	0	-479
25	$NO_2+H \Leftrightarrow NO+OH$	3.50e+14	0	1500
26	$NO_2+O \Leftrightarrow NO+O_2$	1.00e+13	0	600
27	$NO_2+M \Leftrightarrow NO+O+M$	1.10e+16	0	66000

detailed kinetic mechanism including 49 reactive species and 279 elementary reactions (GRI-Mech 2.11 by Bowman et al.) is used. The temperature dependence of the viscosity, the thermal conductivity and the diffusion coefficients are taken into account by linking CHEMIKIN packages (Kee et al., 1986; Kee et al., 1989) with modifications for vector/parallel computations.

Initial distribution of species is assumed to be uniform. High temperature region is given at the center of computational domain as an ignition kernel. The characteristics of initial turbulence field of DNS are listed in Table 2. In Table 2, HR73W and HR132W are hydrogen/air cases, CR36W and CR60W are methane/air cases. To evaluate turbulence intensity effects, ratio of integral scale (l) to the laminar flame thickness (δ_L) is set to be nearly same for each fuel ($l/\delta_L \approx 1.0$ or 2.0). To investigate realization effects on the

Table 2: Numerical parameters for DNS.

ID	Re_λ	Re_l	u'/S_L	l/δ_F	l/δ_L
HR73W	73.3	163.9	2.25	72.8	1.36
HR132W	132.4	296.9	4.17	71.1	1.33
CR36W	36.4	77.5	4.54	17.1	2.20
CR60W	60.1	130.5	7.88	16.6	2.14

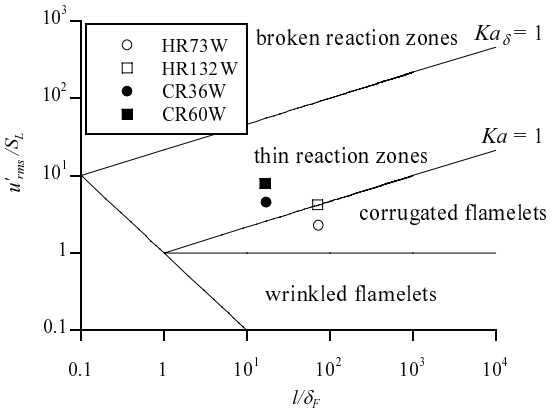

Figure 2: Numerical conditions of the present DNS on the combustion diagram by Peters (1999).

flame-wall interactions, several DNSs are conducted for the statistically same turbulent fields. In Fig. 2, each calculation condition is plotted in the turbulent combustion diagram by Peters (1999). HR132W is located near the boundary between corrugated flamelets and thin reaction zones. HR73W is classified in corrugated flamelets. CR36W and CR60W are classified in thin reaction zones. For comparison, laminar cases were also calculated.

NEAR-WALL BEHAVIOR OF TURBULENT FLAMES

Figures 3 and 4 shows temporal developments of distributions of heat release rate and wall heat flux for hydrogen/air ($Re_\lambda = 132.4$) and methane/air ($Re_\lambda = 60.1$) turbulent premixed flame for T_{wall}=700K. The heat release rate is normalized by the maximum heat release rate (ΔH_L) of corresponding freely-propagating planar laminar flame. Wall heat flux at each wall is shown upper and lower side of distribution of the heat release rate. Heat flux is defined as the product of thermal conductivity coefficient and temperature gradient on the wall. For all cases, flame ignites and propagates in a circular shape on the average from the ignition kernel. However, the flame front is stretched and disturbed its evolution by turbulence. After the flame impinging to the wall, flame propagates along the wall. In this phase, as the expansion effect is caused by the wall bounded field, flame displacement speed toward the no wall direction is higher than that of freely propagating flames.

Since turbulent intensity relative to the laminar burning velocity is high for the methane case ($u'/S_L = 7.88$), geometry of flame front for methane case is complicated compared with that of hydrogen case even though Reynolds number is low for the methane case. High local strain rate causes local extinction and isolated flame islands are created for the methane case.

QUENCHING MECHANISM FROM THE ANALYSES OF CHEMICAL REACTIONS

Figure 5 shows typical distributions of heat release rate

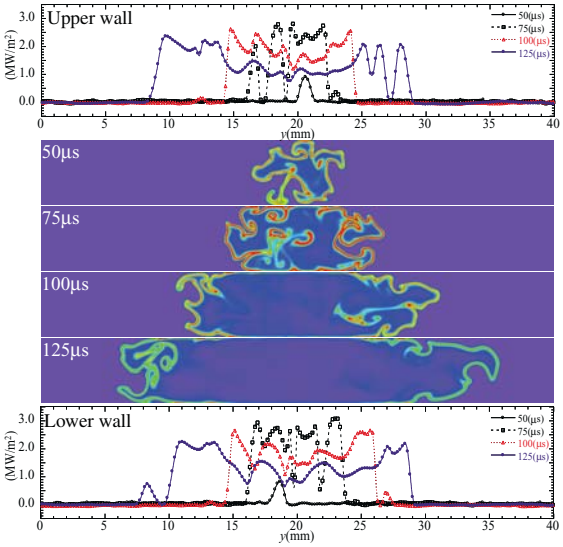

Figure 3: Heat release rate and wall heat flux for hydrogen/air turbulent premixed flame ($Re_\lambda = 132.4$).

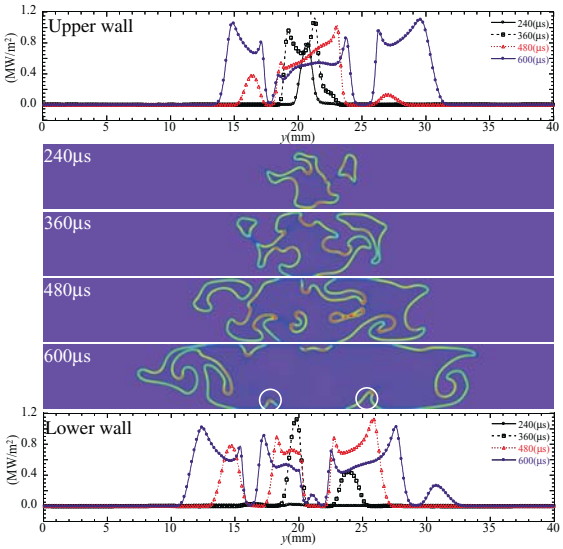

Figure 4: Heat release rate and wall heat flux for methane/air turbulent premixed flame ($Re_\lambda = 60.1$).

near the upper wall for hydrogen/air and methane/air cases. In near-wall region, heat release rate increases drastically for hydrogen cases. This heat release rate is higher than the maximum heat release rate of freely-propagating planar laminar flame (up to $2 \sim 3\Delta H_L$). On the other hand, for methane/air premixed flame, heat release rate decreases in near wall region, and flame quenching occurs.

To investigate the reason why heat release rate near the wall depend on the fuel, elementary reactions were analyzed. Figure 6 shows contributions of major elementary reactions to the total heat release rate in hydrogen/air laminar premixed flame. For hydrogen/air premixed flame, following reactions:

$$\mathrm{R1} : \mathrm{H+O_2 \Leftrightarrow OH+O}$$

$$\mathrm{R3} : \mathrm{H_2+OH \Leftrightarrow H_2O+H}$$

$$\mathrm{R6} : \mathrm{H+O_2 \Leftrightarrow HO_2+M}$$

$$\mathrm{R8} : \mathrm{H+HO_2 \Leftrightarrow OH+OH}$$

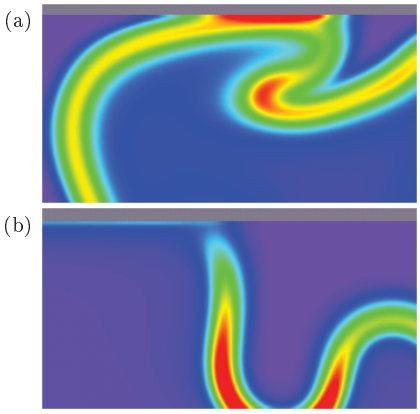

Figure 5: Typical distributions of heat release rate near the wall for hydrogen/air turbulent premixed flame ($Re_\lambda = 132.4$)(a) and for methane/air turbulent premixed flame ($Re_\lambda = 60.1$)(b).

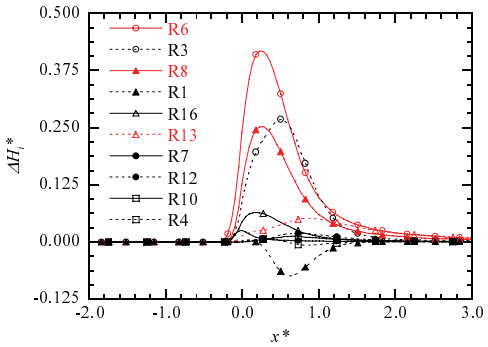

Figure 6: Contributions of major elementary reactions to the total heat release rate in hydrogen/air laminar premixed flame.

$$\mathrm{R16} : \mathrm{H+HO_2 \Leftrightarrow H_2+O_2}$$

have large contribution to the total heat release rate.

Figure 7 shows distribution of heat release rate and reaction rates of R6, R8 and R13 in near-wall region. In Fig. 7, it is clear that these reactions are enhanced and heat release rate is also enhanced in same near-wall region. Because these reactions have low activation energies as shown in Table 1, they are prompted even the low temperature region near the wall. From the detailed analyses of chemical reaction balances, it is concluded that, due to certain low temperature reactions which have large contributions to the total heat release rate and have low activation energies, hydrogen/air premixed flame does not quench near the wall.

The quenching mechanism of the methane/air premixed flame is also analyzed based on the modification of elementary reaction near the wall similar to the hydrogen case. Figure 8 shows contributions of major elementary reactions to the total heat release rate in methane/air laminar premixed flame. For methane/air premixed flame, the following reaction:

$$\mathrm{R10} : \mathrm{CH_3+O \Leftrightarrow CH_2O+H}$$

has the largest contribution to the total heat release rate. Figure 9 shows distribution of heat release rate and reaction rates of R10 and R52 in near-wall region. The reaction rate of R10 decreases in same place where heat release rate decreases near the wall. From the above-mentioned consideration, reaction rate of R10 induces drastic decrease of the

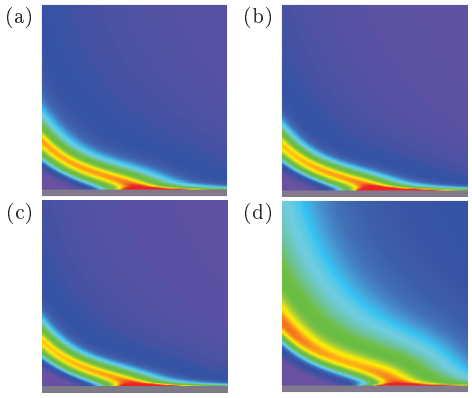

Figure 7: Distributions of heat release rate(a) and reaction rates of R6(b), R8(c) and R13(d) in near-wall region for hydrogen flame.

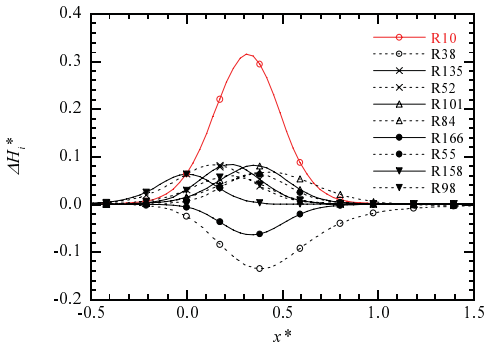

Figure 8: Contributions of major elementary reactions to the total heat release rate in methane/air laminar premixed flame.

heat release rate; i.e. flame quenching near the wall. This decrease of reaction rate of R10 is caused by the R52 reaction as follow:

$$\mathrm{R52 : H{+}CH_3(+M_b) \Leftrightarrow CH_4(+M_b)},$$

which suppresses methane decomposition and is enhanced by the cooling effect near the wall because of its low activation energy. From the discussion based on the reaction mechanism, it is shown that elementary reaction which suppresses methane decomposition is enhanced by the wall cooling effect and induces quenching near the wall.

HEAT TRANSFER ON THE WALL

In laminar cases, the peak of wall heat flux is observed at the time of flame impinges (not shown here), and is 2.5MW/m^2 for hydrogen case and 1.2MW/m^2 for methane case. As for turbulent cases, the maximum heat flux is higher than that of laminar cases for hydrogen flames, whereas the maximum heat flux for methane/air flame does not exceed that of laminar flame as shown in Figs. 3 and 4. Before the flame impinges to the wall, total heat release rate of hydrogen flame is higher than that of methane flame since flame area is larger for hydrogen cases due to high Reynolds number effects. Figure 10 shows density and pressure distributions for hydrogen/air case ($Re_\lambda = 132.4$) at just after the flame impinging to the wall ($t = 75\mu s$). The high total heat release rate induces the adiabatic compression of unburned mixture, which is reflected by the high pressure around the burnt gas. In general, the heat release rate of premixed flame increases for high pressure condition. Therefore,

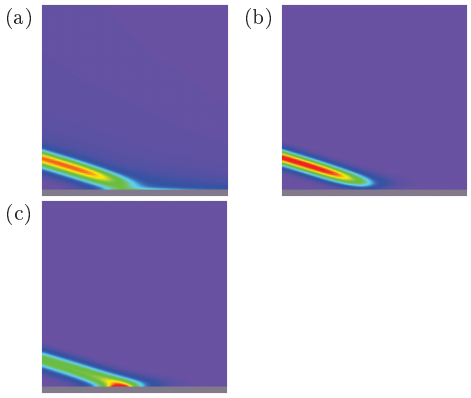

Figure 9: Distributions of heat release rate(a) and reaction rates of R10(b) and R52(c) in near-wall region for methane flame.

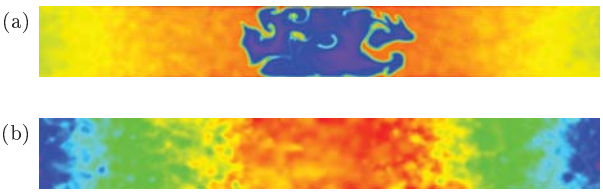

Figure 10: Distributions of density(a) and pressure(b) for hydrogen/air turbulent premixed flame ($Re_\lambda = 132.4$, $t = 75\mu s$).

the maximum heat flux of high Reynolds number hydrogen flame exceeds that of the laminar case. If the flame starts to propagate along the wall, the maximum wall heat flux tends to decrease gradually. For methane cases, since individual isolated flame islands impinge to the wall, the number of attached flame elements is large. The enclosed unburned mixture is consumed slowly due to the low temperature effect near the wall, and the attached points scarcely move and stay at the same location because of the quenching of methane flame (see white circles in Fig. 4). These induce high heat flux in this area over a relatively long time.

Figure 11 shows wall heat fluxes for hydrogen/air turbulent premixed flame ($Re_\lambda = 132.4$) for T_{wall}=450K and 700K. As the wall temperature is lower than preheating temperature for case of T_{wall}=450K, thermal boundary layer develops gradually. In this state, low temperature region near the wall due to the thermal boundary layer is stretched and disturbed by eddies. Because of this thermal boundary layer, heat flux on the wall faced with unburnt mixture also increases, which is reflected by heat flux fluctuation in no flame region (see Fig. 11(b)). Note that instantaneous flame structure is scarcely affected by the wall temperature. As for the maximum heat flux, both cases show almost same value (about 3.0MW/m^2) in spite of difference of wall temperature. This is explained by considering the definition of wall heat flux. Since the difference of the temperature for case of T_{wall}=450K is larger than that for case of T_{wall}=700, temperature gradient for case of T_{wall}=450K is higher than that for the case of T_{wall}=700K. However, coefficient of thermal conductivity for case of T_{wall}=450K is lower than that for case of T_{wall}=700K (not shown here). Therefore, the maximum heat flux becomes nearly same for both cases.

Figure 12(a) shows temporal developments of total heat flux for hydrogen/air case with different Reynolds number for T_{wall}=700K. Here, the total heat flux is defined by the integral of wall heat flux along the wall. Since turbulent

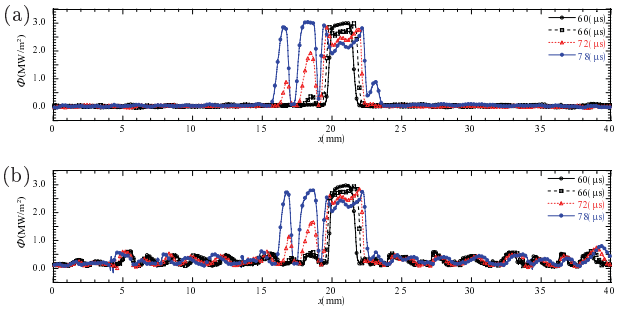

Figure 11: Wall heat flux for hydrogen/air turbulent premixed flame (T_{wall}=700K(a), T_{wall}=450K(b)).

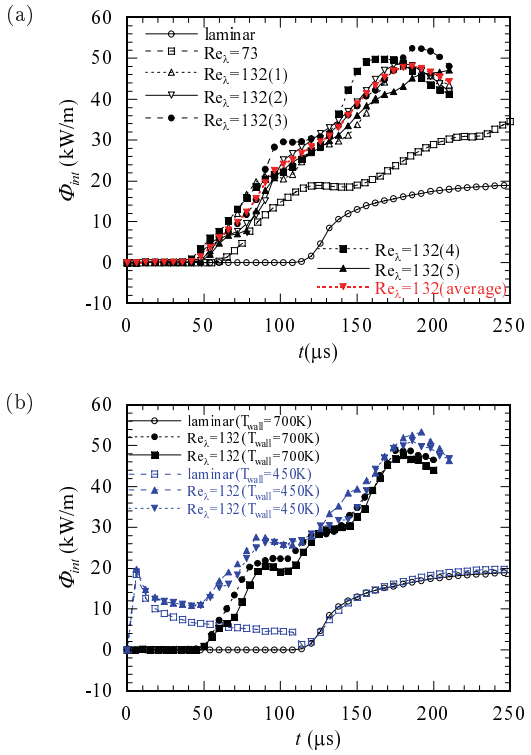

Figure 12: Total wall heat flux for hydrogen/air turbulent premixed flame(different realization(a), different wall temperature(b)).

burning velocity increases with increase of turbulent intensity, the time required for the flame impinging to the wall becomes short for high turbulent intensity case. Therefore, total heat flux increases rapidly for that case. In addition, as the geometry of the flame front becomes complicated and the flame area facing the wall increases for the high turbulent intensity case, the total heat flux becomes higher. Figure 12(b) shows temporal developments of total heat flux for T_{wall}=450K and 700K. Because of heat flux on the wall faced with unburnt mixture due to the thermal boundary layer, the total heat flux for T_{wall}=450K is higher than that for T_{wall}=700K.

To clarify heat loss characteristics, the mean heat transfer rate is introduced. Here, the mean heat transfer rate denotes the average of the heat transfer rate of the wall where flame is attaching the burnt gas. Figure 13 shows temporal developments of mean heat transfer rate for hydrogen/air turbulent premixed flame for T_{wall}=700K. If local flame structure of turbulent flame nearly coincides with that of laminar flame, the maximum mean heat transfer rate

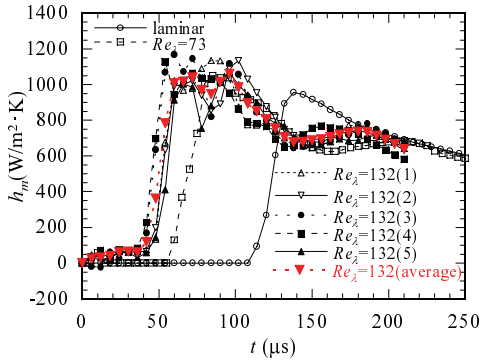

Figure 13: Mean heat transfer rate for hydrogen/air turbulent premixed flame.

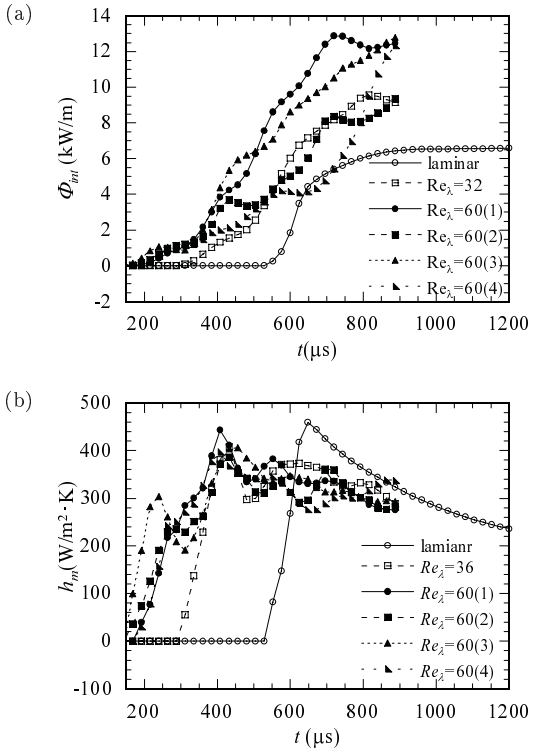

Figure 14: Total wall heat flux(a) and mean heat transfer rate(b) for methane/air turbulent premixed flame.

should be same. However, for turbulent hydrogen flame, it becomes more than 20% higher than that for laminar flame. This is because the heat release rate of each element for turbulent flame increases compared with that for laminar flame if the wall exists as is discussed in the above.

Figure 14(a) shows temporal developments of total heat flux for methane/air premixed flame with different Reynolds number for T_{wall}=700K. From the same reasons for hydrogen/air flame, the total heat flux of turbulent flame is higher than that of laminar flame. However, in mean heat transfer rate (shown in Fig. 14(b)), the maximum value is nearly same with that of laminar flame. This is different from hydrogen flame and seems to be characteristic of hydrocarbon flames.

REALIZATION DEPENDENCE

Figure 15 shows realization dependence of heat release rate for hydrogen/air turbulent premixed flame (Re_λ = 132.4 and T_{wall}=700K). Even for the statistically same tur-

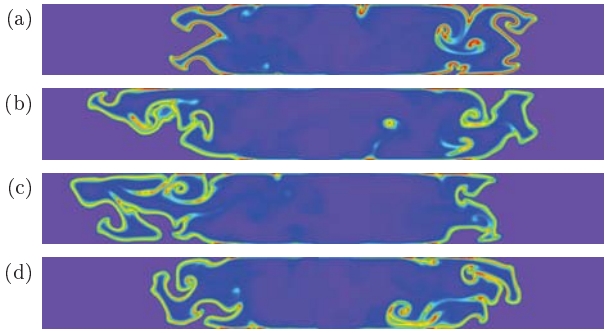

Figure 15: Distributions of heat release rate of different realizations for hydrogen/air turbulent premixed flame ($Re_\lambda = 132.4$, $t = 120\mu s$).

bulence, flame structure strongly depends on the ignition point. In Fig. 12(a), total heat flux obtained for different realizations for $Re_\lambda = 132.4$ are also shown. Although the instantaneous flame structure strongly depends on the ignition point in turbulence, the total heat flux shows almost same trends for all cases. As for the mean heat transfer rate, realization dependence is also weak (see Fig. 13). This fact suggests that the dominant parameter which determines the heat loss is turbulence characteristics for hydrogen/air turbulent premixed flame.

For methane cases, however, the trend of the total heat flux and mean heat transfer rate for different realization (see Fig. 14) is greatly different even for the same turbulence condition. This seems to be related to the flame quenching and the lower turbulent burning velocity for methane flame compared with hydrogen flame.

CONCLUSION

In this study, direct numerical simulations of interactions between turbulent premixed flame and isothermal wall have been conducted.

For hydrogen/air turbulent premixed flame, heat release rate increases in near-wall region and the flame does not quench. The reason for no occurrence of flame quench was discussed based on the elementary reaction. For methane/air turbulent premixed flame, because of suppression of the decomposition reaction near the wall, heat release rate decreases in near-wall region and the flame quenching occurs.

For high intensity hydrogen/air turbulent premixed flame, since heat release rate of whole flame front is increased for wall bounded geometry, heat flux at wall and mean heat transfer rate exceed those of laminar flame. Due to the flame quenching near the wall, mean heat transfer rate for methane/air turbulent premixed flame nearly coincides with laminar case even though the total heat flux increases.

ACKNOWLEDGMENTS

This work is partially supported by Grant-in-Aid for Scientific Research (S) (No.18106004) of Japan Society for the Promotion of Science.

REFERENCES

Baum, M., Poinsot, T. and Thevenin, D., 1994, "Accurate Boundary Conditions for Multicomponent Reactive Flows", *Journal of Computational Physics*, Vol. 106, pp. 247-261.

Bellenoue, M., Kageyama, T., Labuda, S. A., Sotton, J., 2003, "Direct Measurement of Laminar Flame Quenching Distance in a Closed Vessel", *Experimental Thermal and Fluid Science*, Vol. 27, pp. 323-331.

Boust, B., Sotton, J., Labuda, S. A., Bellenoue, M., 2007, "A Thermal Formulation for Single-wall Quenching of Transient Laminar Flames", *Combustion and Flame*, Vol. 149, pp. 286-294.

Bowman, C. T., Hanson, R. K., Davidson, D. F., Gardliner Jr., W. C., Lissianski, V., Smith, G. P., Golden, D. M., Frenklach, M. and Goldenberg, M., *Available from: http://www.me.berkeley.edu/ gri_mech.*

Brown, P. N., Byrne, G. D. and Hindmarsh, A. C., 1989, "VODE, A Variable-coefficient ODE Solver", *SIAM Journal on Scientific and Statistical Computing*, Vol. 10, pp. 1038-1051.

Dabireau, F., Cuenot, B., Vermorel, O. and Poinsot, T., 2003, "Interaction of Flames of H_2+O_2 With Inert Walls", *Combustion and Flame*, Vol. 135, pp. 123-133.

Kee, R. J., Dixon-Lewis, G., Warnatz, J., Coltrin, M. E. and Miller, J. A., 1986, "A Fortran Computer Code Package for the Evaluation of Gas-Phase Multicomponent Transport Properties", *Sandia Report*, SAND86-8246.

Kee, R. J., Rupley, F. M. and Miller, J. A., 1989, "Chemkin-II: A Fortran Chemical Kinetics Package for the Analysis of Gas Phase Chemical Kinetics", *Sandia Report*, SAND89-8009B.

Kee, R. J., Rupley, F. M., Meeks, E. and Miller, J. A., 1996, "Chemkin-III: A Fortran Chemical Kinetics Pacage the Analysis of Gas-phase Chemical and Plasma Kinetcs", *Sandia Report*, SAND96-8216.

Lele, S. K., 1992, "Compact Finite Difference Schemes with Spectral-like Resolution", *Journal of Computational Physics*, Vol. 103, pp. 16-42.

Miller, J. A. and Bowman, C. T., "Mechanism and Modeling of Nitrogen Chemistry in Combustion", *Progress in Energy and Combustion Science*, Vol. 15, pp. 287-338.

Miyauchi, T., Tanahashi, M., Sasaki, K. and Ozeki, T., 1996, "Transport Phenomena in Combustion", Chen, C. H. ed., Taylor and Francis, New York, pp. 1095-1105.

Owston, R., Magi, V. and Abraham, J., 2007, "Interactions of Hydrogen Flames With Walls: Influence of Wall Temperature, Pressure, Equivalence Ratio, and Diluents", *International Journal of Hydrogen Energy*, Vol. 32, pp. 2094-2104.

Peters, N., 1999, "The Turbulent Burning Velocity for Large-Scale and Small-Scale Turbulence", *Journal of Fluid Mechanics*, Vol. 384, pp. 107-132.

Poinsot, T. J. and Lele, S. K., "Boundary Conditions for Direct Simulations of Compressible Viscous Flows" *Journal of Computational Physics*, Vol. 101, pp. 104-129, (1992).

Popp, P. and Baum, M., 1997, "Analysis of Wall Heat Fluxes, Reaction Mechanisms, and Unburnt Hydrocarbons during the Head-on Quenching of a Laminar Methane Flame", *Combustion and Flame*, Vol. 108, pp. 327-348.

Smooke, M. D. and Giovangigli, V., 1991, "Formulation of the Premixed and Nonpremixed Test Problems", *Reduced Kinetic Mechanisms and Asymptotic Approximations for Methane-Air Flames, Springer-Verlag*, pp. 1-28.

Tanahashi, M., Fujimura, M. and Miyauchi, T., 2000, "Coherent Fine-Scale Eddies in Turbulent Premixed Flames,", *Proceedings of the Combustion Institute*, Vol. 28, pp. 529-535.

Tanahashi, M., Nada, Y., Ito, Y. and Miyauchi, T., 2002, "Local Flame Structure in the Well-Stirred Reactor Regime", *Proceedings of the Combustion Institute*, Vol. 29, pp. 2041-2049.